Neuro-Oncology Advances

3(1), 1–9, 2021 | https://doi.org/10.1093/noajnl/vdab088 | Advance Access date 24 June 2021

Analysis of morphological characteristics of IDH-mutant/wildtype brain tumors using whole-lesion phenotype analysis

James M. Snyder, Raymond Y. Huang, Harrison Bai, Vikram R. Rao, Susannah Cornes, Jill S. Barnholtz-Sloan, David Gutman, Rebecca Fasano, Erwin G. Van Meir, Daniel Brat, Jennifer Eschbacher, John Quackenbush, Patrick Y. Wen, and Jong Woo Lee

Departments of Neurosurgery and Neurology, Henry Ford Health System, Detroit, Michigan, USA (J.M.S.); Department of Radiology, Brigham and Women's Hospital, Harvard Medical School, Boston, Massachusetts, USA (R.Y.H.); Department of Diagnostic Imaging, Rhode Island Hospital and Warren Alpert Medical School of Brown University, Providence, Rhode Island, USA (H.B.); Department of Neurology and Weill Institute for Neurosciences, University of California, San Francisco, San Francisco, California, USA (V.R.R., S.C.); Department of Population and Quantitative Health Sciences, School of Medicine Case Western Reserve University and University Hospitals of Cleveland, Cleveland, Ohio, USA (J.S.B.-S.); Winship Cancer Institute, Emory University, Atlanta, Georgia, USA (D.G.); Department of Neurology, Emory University, Atlanta, Georgia, USA (R.F.); O'Neal Comprehensive Cancer Center, University of Alabama at Birmingham (UAB), Birmingham, Alabama, USA (E.G.V.M.); Department of Pathology, Feinberg School of Medicine, Northwestern University, Chicago, Illinois, USA (D.B.); St. Joseph's Hospital and Medical Center, Phoenix, Arizona, USA (J.E.); Department of Biostatistics, Harvard T.H. Chan School of Public Health, Center for Cancer Computational Biology, Dana Farber Cancer Institute, Boston, Massachusetts, USA (J.Q.); Center for Neuro-Oncology, Dana-Farber Cancer Institute, Boston, Massachusetts, USA (P.Y.W.); Department of Neurology, Brigham and Women's Hospital, Harvard Medical School, Boston, Massachusetts, USA (J.W.L.)

Corresponding Author: Jong Woo Lee, MD, PhD, Department of Neurology, Brigham and Women's Hospital, 60 Fenwood Road, Boston, MA 02115, USA (jlee38@bwh.harvard.edu).

Abstract

Background. Although IDH-mutant tumors aggregate to the frontotemporal regions, the clustering pattern of IDH-wildtype tumors is less clear. As voxel-based lesion-symptom mapping (VLSM) has several limitations for solid lesion mapping, a new technique, whole-lesion phenotype analysis (WLPA), is developed. We utilize WLPA to assess spatial clustering of tumors with IDH mutation from The Cancer Genome Atlas and The Cancer Imaging Archive.

Methods. The degree of tumor clustering segmented from T1 weighted images is measured to every other tumor by a function of lesion similarity to each other via the Hausdorff distance. Each tumor is ranked according to the degree to which its neighboring tumors show identical phenotypes, and through a permutation technique, significant tumors are determined. VLSM was applied through a previously described method.

Results. A total of 244 patients of mixed-grade gliomas (WHO II–IV) are analyzed, of which 150 were IDH-wildtype and 139 were glioblastomas. VLSM identifies frontal lobe regions that are more likely associated with the presence of IDH mutation but no regions where IDH-wildtype was more likely to be present. WLPA identifies both IDH-mutant and -wildtype tumors exhibit statistically significant spatial clustering.

Conclusion. WLPA may provide additional statistical power when compared with VLSM without making several potentially erroneous assumptions. WLPA identifies tumors most likely to exhibit particular phenotypes, rather than producing anatomical maps, and may be used in conjunction with VLSM to understand the relationship between tumor morphology and biologically relevant tumor phenotypes.

Key Points

- Spatial clustering patterns of IDH-wildtype tumors are not as well defined as IDH-mutant tumors.
- Voxel-based lesion-symptom mapping has limitations in solid lesion analysis; whole-lesion phenotype analysis (WLPA) is an alternate method that overcomes some of these limitations.
- We utilize WLPA to demonstrate the existence of statistically significant spatial clustering of both IDH-mutant and -wildtype brain tumors.

Importance of Study

Voxel-based lesion-symptom mapping (VLSM) has been utilized to demonstrate the clustering of IDH-mutant tumors to the frontotemporal regions. Although VLSM identifies a relationship between anatomical structures and phenotype, it makes certain assumptions that may render it less applicable to solid lesions. We developed an alternate method of assessing spatial clustering, the whole-lesion phenotype analysis (WLPA). We demonstrate the utility of this technique in revealing that IDH-wildtype tumors tend to exhibit spatial clustering, which was not observed with VLSM. We hypothesize that the smaller IDH-wildtype tumors result in anatomically sparse distribution, rendering VLSM less effective than WLPA. Although it does not produce statistical maps like VLSM, WLPA identifies IDH-wildtype tumors that are most likely to be spatially associated with other IDH-wildtype tumors. WLPA may be utilized in conjunction with VLSM to assess the relationship between tumor morphology and biologically relevant tumor phenotypes.

Spatial clustering of IDH-mutant brain tumors has been demonstrated by multiple studies. IDH-mutant tumors tend to aggregate to the frontal or temporal lobes.[1–3] Some of the technically most advanced studies have utilized the voxel-based lesion-symptom mapping (VLSM)[4] or similar anatomical mapping techniques, which allows for the assessment of lesions demonstrating a critical relationship between anatomical structure and clinical function. Although initially developed to map clinical symptoms based on lesion location, VLSM has been adapted to perform a more general lesion phenotype mapping, including those caused by brain tumors.[5,6]There are several benefits to this technique:

1. It requires no artificial anatomical boundaries that are frequently not respected by a given lesion.
2. It does not require a priori region of interest delineation.
3. It provides a statistical map of anatomical regions that are associated with a particular phenotype.

However, there are shortcomings to this methodology, some of which are specific to solid lesion imaging:

1. There is an uneven spatial distribution of statistical power; a relatively large number of lesions are required to ensure that a biologically significant region attains a sufficient number of voxels.[7] In extreme cases, lesions that do not have spatial overlap with other lesions are not informative and do not contribute to statistical power. However, such lesions may still be informative. For example, the presence of multiple nonoverlapping lesions of a single phenotype over a specific anatomical region strongly suggests an association between that region and the phenotype.
2. There is an assumption of independence of voxels contributing to the association with a phenotype, that is, that any spatial location vulnerable to a lesion of a particular phenotype is equally likely to be affected.[8,9]
3. There is also an assumption of spatial independence, that is, that the phenotype of one voxel is independent of the phenotype of other voxels. This is not likely the case in solid lesions, especially since there is a robust spatial correlation for any given phenotype. More insidiously, if voxels of certain anatomical locations that are not biologically associated with a particular phenotype are nonetheless frequently associated with a particular phenotype only as a result of anatomical continuity with voxels that are biologically associated with the phenotype, this may lead to the erroneous discovery that a specific brain location is statistically associated with a particular phenotype.[5]
4. Phenotypes, particularly clinical ones, are complex and may draw on several structural/morphological characteristics; the anatomical location is typically only one of many determinants. Even within the radiographic realm, several features of lesion morphology may play significant roles.

Although these reasons may render lesion-based mapping methods to be generally difficult to interpret and may lead to conflicting or unexpected negative results,[10–12] lesion mapping strategies may still offer insight into lesions associated with phenotypes. Rather than attempting to determine whether phenotypes map to specific brain regions, we propose an alternate approach to determine whether lesions with predefined measures, such as morphological similarity, results in a characteristic phenotype.

Here we describe a simple new analysis technique, whole-lesion phenotype analysis (WLPA). The underlying principle of this analysis is that there is a clustering of lesions associated with a particular phenotype or genotype and that a function of lesion similarity measures the degree of clustering. We then rank each of the lesions according to the degree to which its neighboring lesions show an identical phenotype. Through a permutation technique, we determine which of these lesions are significantly clustered. Thus, we attempt to analyze on a lesion basis, rather than mapping based on brain anatomy, which in certain situations may overcome some of the issues with VLSM. We demonstrate this method using The Cancer Genome Atlas (TCGA) dataset of brain tumors by focusing on a genotype of interest: IDH-wildtype versus mutant. We test the hypothesis that tumors display distinct clustering characteristics according to phenotype. Although one may infer anatomical location, this is not the basis of the analysis.

Materials and Methods

Patients and Scans

Patients were identified through TCGA glioblastoma multiforme (GBM) and lower-grade glioma (LGG) datasets and cross-referenced with MRI from The Cancer Imaging Archive (TCIA). Both the GBM and LGG datasets were utilized. IDH1/2 mutational status was obtained from TCGA. All patients with IDH mutational data and preoperative MRI scans were included.

Image Processing

Tumors were manually segmented from the MRI by blinded raters using standard image processing software (3D Slicer, www.slicer.com). The tumor margin was delineated by either the area of contrast enhancement or, if nonenhancing, the extent of the abnormal signal on T1-weighted images. Tumor margins were also delineated by the extent of abnormal signal on T2-weighted images for confirmatory analysis.

MR images were transformed into a standardized coordinate space based on the Talairach atlas[13] to account for differences in brain orientation and intracranial volume. Automatic registration using linear affine transformation was performed from the T1-weighted images.[14] Because distortions of the anatomy caused the registration procedure to fail at times, registration validity was checked by selecting 6 points on both the template and the target brains (maximal anterior and posterior cortical extent along the anterior–posterior commissure (AC-PC) line, upper and lower extent along the perpendicular line through the AC; left and right extent along the third axis formed by the 2 previous lines). If the root mean square is greater than 5 mm, registration was reperformed using the manually selected coordinates. Tumor volumes were calculated after registration (MATLAB, Mathworks, Natick, MA). The dataset and Matlab code are available on request.

Statistical Analysis

Anatomical Statistical Mapping

Tumor masks were then used to determine the regions where patients were more likely to present with or without IDH mutation using a previously described voxel-wise method adapted to solid lesions.[15] Briefly, a χ^2 statistic map was calculated at each voxel to determine the deviation from the expected number of IDH-mutant tumors at that voxel when compared with the overall population. In voxels where the number of patients with IDH mutation exceeded the number of patients without IDH mutation, a higher value of χ^2 is indicative of a stronger likelihood that patients with a tumor at that location would present with IDH mutation than at other locations. A complementary χ^2 map was calculated to determine locations where presentation with IDH mutation was less likely. The significance of the χ^2 statistic was then determined by a clustering and nonparametric resampling method. Signal clusters were obtained through a 6-connectivity model.[16] To determine the significant clusters without making arbitrary assumptions regarding cluster strength threshold, the threshold-free cluster enhancement (TFCE) technique was first applied.[17] Thereafter, the labeling of each patient as IDH-mutant versus wildtype was randomly reassigned, with the constraint of preserving the original ratio. From the relabeled group, a χ^2-statistic map and TFCE scores were calculated, and the maximum TFCE score across all voxels was recorded. This was repeated 5000 times to obtain a null hypothesis distribution of maximal TFCE.[16,18] Clusters of the original image whose TFCE scores exceeded significance of $P < .05$ were considered significant.

Whole-Lesion Phenotype Analysis

The basic steps are as follows and are adapted from a previous methodology measuring differential gene expression of 2 phenotypes:[19]

1. The similarity score is calculated as follows: between each pair of lesions, the Hausdorff distance,[20,21] a robust measure of similarity between 2 images, was calculated. Simply, the Hausdorff distance between 2 sets of planes is calculated by obtaining the set of minimum distances from every point of one plane to the other and then selecting the maximum of that set (eg, Figure 1). To derive a relatively linear unit score (eg, scores between 0 and 1), the exponential of the negation of the Hausdorff distance was utilized as the similarity score ($H_{1..i}$).

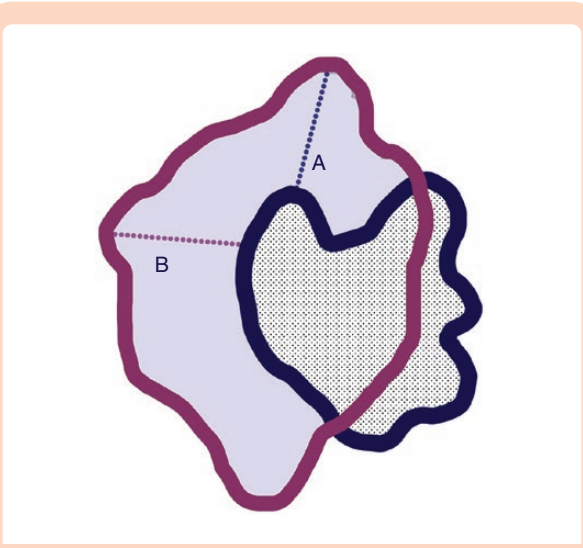

Figure 1. Example of Hausdorff distance calculation. Line A represents the maximum of the set of minimum distance from blue to red lesion, and line B represents the maximum of the set of minimum distance from red to blue lesion. The Hausdorff distance is the greater of A and B.

An index of tumor volume overlap in space was calculated, as it would have been a reasonable proxy of tumor similarity. For tumors A and B:

$$I = \frac{2*(A \cap B)}{A \cup B}$$

Nonzero values had a high correlation with the transformed Hausdorff distance (ρ = 0.59). The Hausdorff distance was utilized as a measure of similarity as it has the distinct advantage of every pair of tumors being informative, whereas nonoverlapping pairs are minimally informative with the overlap index.

2. For each lesion (index lesion), all other lesions are ordered in decreasing similarity. Thereafter, an enrichment score (ES) is calculated as follows: if the next closest lesion encountered has the same phenotype, the ES is increased by

$$\frac{H_{i\hat{}p}}{N_{\text{same}}}$$

where N_{same} is the sum of $H_{g\hat{}p}$ where g is the subset of all lesions that have the same phenotype as the index lesion (Supplementary Figure).

3. If the lesion encountered has the opposite phenotype, the score is decreased by $\frac{1}{N_{\text{diff}}}$ where N_{diff} is the number of all the lesions whose phenotype is different than the index lesion. The omnibus statistic is the maximum ES for all lesions in the dataset. If the exponential $p = 0$, this reduces the ES to the Kolmogorov–Smirnov (K-S) statistic. If $p = 1$, this is an enriched K-S statistic.

4. The membership of the phenotype is permuted while keeping the total number of members in each phenotype the same. For each permutation, the maximum ES is calculated, and the distribution of ES is obtained. The original lesions that fall outside 95% of the permutated distribution are considered significant.

The primary analysis was performed using T1-weighted images. Because of the inevitable variability in demarcating the tumor, analyses were also performed utilizing T2-weighted images; and utilizing T1-weighted images for glioblastomas and T2/FLAIR images for LGGs.

Analysis was performed using MATLAB R2015b (Mathworks, Natick, MA). Rendering was performed on MRIcron.[7] The local institutional review board approved this study.

Results

A total of 330 patients were included. Of these, the IDH status was available in 244 patients (150 IDH-wildtype, 94 IDH-mutated). Deceased patients were older at the time of study than alive patients, and IDH-wildtype patients were older than IDH-mutant patients (Table 1). The normalized volume of patients with "deceased" status was smaller than patients who were alive (Table 1). The tumor volume of patients with IDH-mutant tumors was larger than IDH1-wildtype tumors. There was no difference in gender (Table 1). The aggregate maps of all IDH-wildtype and IDH-mutant tumors are shown in Figure 2 across 3 axial slices.

Anatomical Statistical Mapping (VLSM)

Statistical mapping to determine regions with significantly more tumors with IDH mutation status revealed 2 significant clusters, both in the deep right/midline frontal region: the first was of size 62.3 cc^3 and maximal χ^2 of 29.05, while the second was of size 0.17cc^3 with maximal χ^2 of 14.6. No significant regions with more tumors with IDH-wildtype were found (Table 2).

Whole-Lesion Phenotype Analysis

Figure 3 illustrates the heat map of the ESs, visually demonstrating that tumors with high ESs tend to cluster. There appear to be unexpected clusters of tumors with low ESs, suggesting the existence of potential distant secondary clusters.

A total of 35 IDH-wildtype tumors and 28 IDH-mutant tumors showed statistically significant aggregation to tumors of the same phenotype when assessed by the tumor similarity score when compared with a random distribution. Visual assessment of the distribution of these tumors revealed that IDH-mutant tumors clustered more anteriorly, with greater involvement of the insular cortex, whereas the IDH-wildtype tumors clustered more posteriorly.

The IDH-mutant tumor with the greatest ES (TCGA code FG-A4MT, P = .001) is the same left frontal lower-grade glioma previously described. This tumor can be considered

Table 1. Demographics

Variable	IDH-Mutant	IDH-Wildtype	Statistic
Total patients	94	150	
Mean age (SD)	42.5 (13.3)	62.7 (11.4)	$P < .0001$
Female (%)	38 (40.9%)	62 (41.1%)	$P =$ NS
The Cancer Genome Atlas database			$P < .0001$
Glioblastoma multiforme (%)	10 (10.8%)	128 (85. 3%)	
Lower-grade glioma (%)[a]	83 (89.3%)	22 (14.7%)	
Grade 2 (%)	43 (45.7%)	7 (4.7%)	
Grade 3 (%)	39 (41.5%)	15 (10.0%)	
Tumor volume cc^3 (SD)	89.7 (81.1)	45.1 (33.0)	$P < .0001$

[a]One patient with IDH mutation had discrepant grade.

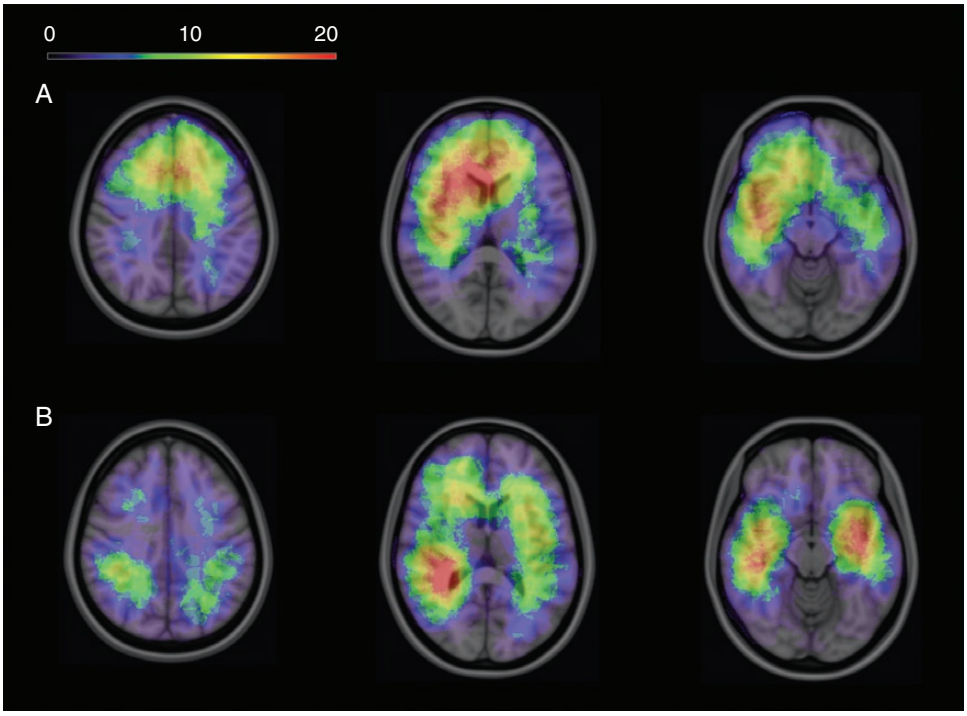

Figure 2. Aggregate tumor map for (A) IDH-mutant and (B) IDH-wild type. Colormap represents aggregate number of patients at each voxel.

Table 2. Regions More Likely to be IDH-Mutant

Region	Size (cc^3)	χ^2 Max	Voxel/Talairach Coordinates
Right/midline anterior frontal	62.3	29.1	90, 163, 83/1, 36, 10
Right/midline anterior frontal	0.17	14.6	72, 184, 100/19, 57, 27

as having the greatest similarity with other IDH-mutant tumors for the given metric. The IDH-wildtype tumor with the greatest ES (TCGA code 19-4068, $P = .0009$) is a small left occipital GBM. Figure 4 shows the aggregate cluster maps of IDH-mutant (4B) and wildtype tumors (4C) that reached significance, along with the 5 tumors with the greatest ES.

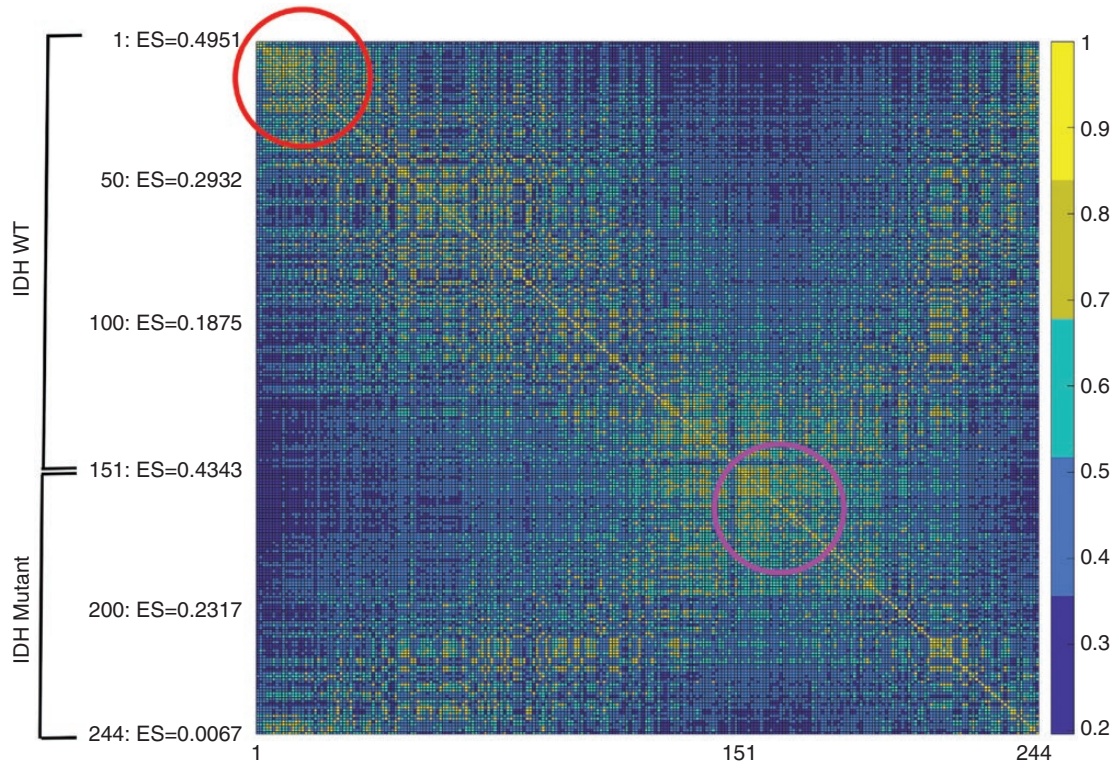

Figure 3. Heat map of the Hausdorff distances, ordered by descending enrichment scores. Tumors 1–150 are IDH-wild type, and 151–244 are IDH-mutant. Tumors clusters are visually apparent, both for IDH-wild type (red circle) or IDH-mutant (purple circle).

The analysis performed utilizing T2/FLAIR resulted in 20 significant tumors (12 IDH-mutant, 8 wildtype), most of which were a subset of the tumors significant on the T1-significant tumor set (80%; 9 of 12 for IDH-mutant, 7 of 8 for IDH-wildtype). The analysis performed utilizing T1-weighted images for glioblastomas and T2/FLAIR images for LGG resulted in a set of 52 significant tumors (28 IDH-mutant, 24 IDH-wildtype), again most of which were a subset of the T1-significant tumor set (77%, 40 of 52 IDH-mutant, 20 of 24 IDH-wildtype).

Discussion

We analyze the association of anatomical characteristics of individual brain tumors based on MR images of a genotype of interest, IDH mutational status, using 2 different analysis techniques, VLSM and WLPA. VLSM represents a robust and powerful technique in determining anatomical correlates with phenotype and has been utilized in several studies, including brain tumors, but makes several key assumptions that may result in both misleading positive findings and potentially underpowering others.[22,23] Here, we introduce a new WLPA technique that overcomes some of these limitations by analyzing the clustering of tumors based on tumor similarity, though it does not produce a traditional statistical map.

IDH-Mutant Versus Wildtype

We redemonstrate that tumors with IDH mutations have a predilection for a frontal lobe location using a modification of the VLSM method, a finding previously demonstrated in multiple studies. The location of the statistically significant clusters was virtually identical to the map produced by the study by Tejada Neyra et al., in particular.[1,2] However, our VLSM results, consistent with previous studies, failed to demonstrate any anatomical aggregation for IDH-wildtype tumors. Using the WLPA, we demonstrate that there is a statistically significant aggregation of IDH-mutant tumors in the frontal region; in addition, we also determined significant aggregation of IDH-wildtype tumors as well. Thus, we established that the distribution of IDH-wildtype tumors is not random and exhibits spatial clustering.

The possible influence of IDH mutations on tumor clinical behavior has led to investigations of the relationship between the location and shape of gliomas employing neuroimaging methods.[24,25] Previous studies have found that gliomas with IDH mutations tend to be located within the frontal or temporal lobes but are rarely seen in the diencephalon or brain stem.[3] In correlation analyses between the IDH status and tumor location applying boundaries of the frontal, parietal, occipital, insular, or temporal lobe, prior studies found that tumors located in insular, frontal, and temporal lobes presented

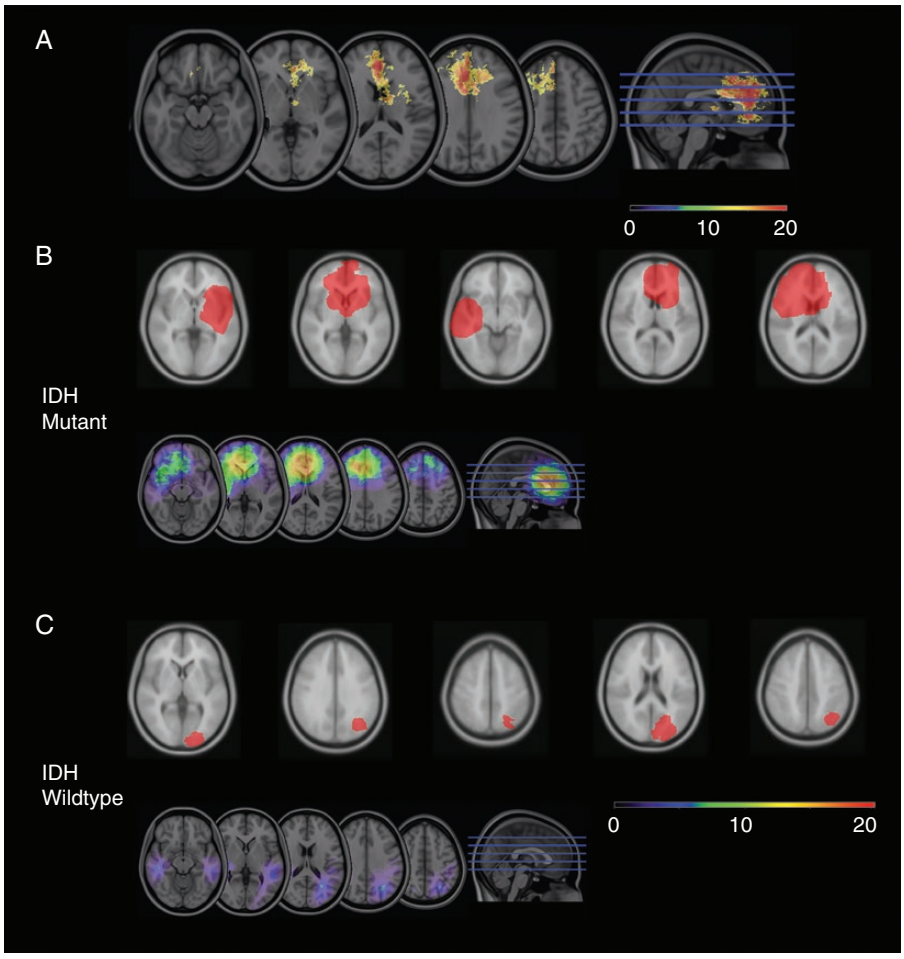

Figure 4. (A) Regions of statistical significance for tumors with IDH mutation using VLSM. Colormap represents the associated X^2 values; (B) and (C) Analysis utilizing WLPA. (B) Tumors with IDH mutation. (Upper) Locations of tumors, in order, with the 5 highest ES. (Lower) Aggregate sum map of all IDH-mutant tumors that reached statistical significance. (C) Tumors with IDH-wild type. (Upper) Locations of tumors, in order, with the 5 highest ES. (Lower) Aggregate sum map of all tumors with IDH-wild type that reached statistical significance.

with frequent IDH mutation rates which were 100%, 89%, and 72%, respectively, and tumors infiltrating the frontal lobe were associated with IDH1 or IDH2 mutations.[3] It has been proposed that most gliomas originate from a population of neural stem/progenitor cells, which are isolated from the subventricular zone in the lining of the lateral ventricles.[26,27] Although the involvement of the subventricular zone is not apparent in the IDH-mutant aggregate images, this is more apparent with the significant images produced by WLPA. The clustering tumor areas we found are also coincident with the localization pattern of gliomas with combined deletions of 1p and 19q,[28] which are associated with IDH1/2 mutations.[29]

Some studies report greater volume in IDH-wildtype WHO grade II gliomas,[30] which seems in conflict with our findings of larger tumor volumes in the IDH-mutated group, though the latter cohort included GBM patients. IDH mutations induce supraphysiologic D-2-hydroxyglutarate levels, which are thought to result in epigenetic dysfunction, dysregulation of multiple enzymes, and pathways shown to contribute to oncogenesis, and when induced in the subventricular zone of a murine model, results in proliferative tumor nodules with brain infiltrating cells harboring subventricular zone markers.[31,32] IDH-mutant tumors have shown a proclivity for the frontal lobes, a neuroanatomical site with a greater tolerance for mass effect than other regions, which may result in delayed tumor identification. Previous studies also note younger age of IDH-mutant groups, which is in agreement with our findings (though not significant in our cohort), might also contribute to the larger volumes of tumors.[3]

Analysis Strategy

We demonstrate a new analysis strategy, WLPA, which was compared with a traditional voxel-based mapping method. The advantage of this system is demonstrated in the fact that the voxel-based mapping method did not produce any

significant results for IDH-wildtype tumors, whereas WLPA was able to detect clustering in this group. This was most likely because, in certain regions, the anatomical distribution is relatively sparse, resulting in few voxels over those regions that are still highly significant. The IDH-wildtype tumors had substantially lower tumor volumes than IDH-mutant tumors, likely contributing to this finding. Although this does not present an obstacle in studies where every voxel is informative, such as fMRI experiments, it likely lowers statistical power in any study involving solid lesion mapping.

There are some limitations in our study, particularly on our statistical techniques.

1. Two datasets of the same size drawn from similar populations examining the same phenotype will necessarily result in a differing set of significant lesions that aggregate. By the nature of the technique, the statistically significant clustering lesions will not be identical in both data sets. However, differences in underlying statistical maps can be expected with any mapping technology.
2. The technique will not result in a visually distinct map. However, we believe that these types of maps may be misleading, particularly when applied to solid lesions. Examination of the statistically significant clustering lesions can be used to inference more biologically relevant hypotheses as to why these lesions resulted in the phenotype, of which spatial location may indeed be the reason.
3. We have limited ourselves to the analysis of a tumor phenotype, which is potentially simpler to analyze than symptom phenotype. Our study could be strengthened with additional analysis of clinically relevant tumor markers, including IDH-mutant subtypes such as 1p19q status and glioma-CpG Island methylator phenotype,[33] as well as symptom phenotypes such as performance status, seizure control, and neurologic deficits that impact quality of life. In addition to the issues raised, symptom mapping probably needs to take into account the nonlocal effects of tumors.[34,35]
4. We have used the Hausdorff distance as a measure of spatial similarity between any 2 lesions. It is conceptually sound and easy to calculate, accounting for both spatial location as well as gross morphology of the lesion. Nonetheless, it likely does not capture the full complexity of potential spatial similarity measures.
5. Analysis with a confirmatory dataset may provide further evidence of the external validity of the presented results.

Conclusion

We demonstrate a novel technique, WLPA, to identify anatomic clustering based on IDH mutation status using radiographic images from a large public database. WLPA addresses some limitations of VLSM's underlying assumptions that may limit its ability to detect true clusters as well as falsely detect localizing anatomical regions. A difference of WLPA when compared with VLSM is that it identifies tumors most likely to exhibit particular phenotypes or genotypes, rather than producing anatomical maps. Thus, these methods may be complementary in establishing the relationship between tumor morphology and biologically relevant clinical and tumor behavior.

Supplementary Data

Supplementary data are available at *Neuro-Oncology Advances* online.

Keywords

brain tumor | IDH mutation | statistical mapping | TCGA | TCIA

Funding

National Institute for Neurologic Disorders and Stroke (R03 NS091864 to J.L.).

Conflict of interest statement. J.W.L: Contract work for Bioserenity, Teladoc. Co-founder, Soterya Inc. D.G.: Scientific Advisory Board for HistoWiz, LLC. P.W.: (1) Research Support: Agios, Astra Zeneca/Medimmune, Beigene, Celgene, Eli Lily, Genentech/Roche, Kazia, MediciNova, Merck, Novartis, Nuvation Bio, Oncoceutics, Vascular Biogenics, VBI Vaccines. (2) Advisory Board: Agios, Astra Zeneca, Bayer, Boston Pharmaceuticals, CNS Pharmaceuticals, Elevate Bio Immunomic Therapeutics, Imvax, Karyopharm, Merck, Novartis, Nuvation Bio, Vascular Biogenics, VBI Vaccines, Voyager, QED, Celularity, Sapience. V.R.: Supported by the Ernest Gallo Distinguished Professorship at the University of California, San Francisco; Consultant for NeuroPace, Inc., not relevant to this study. J.Q.: NIH 1R35CA22052, 5U24CA194354. E.G.V.M.: NIH R01 CA235162, NS096236, Department of Defense CA170948, B*Cured Foundation and CURE Childhood Cancer Foundation. J.M.S., R.Y.H., H.B., S.C., J.S.B.-S., R.F., D.B., and J.E. have nothing to declare.

Authorship Statement. Design: J.M.S., V.R.R., S.C., J.S.B.-S., R.F., J.E., J.Q., P.Y.W., J.W.L. Implementation: J.M.S., R.Y.H., H.B., V.R.R., S.C., J.S.B.-S., D.G., R.F., E.G.V.M., D.B., J.E. Analysis and interpretation: J.M.S., J.Q., J.W.L.

References

1. Ellingson BM, Lai A, Harris RJ, et al. Probabilistic radiographic atlas of glioblastoma phenotypes. *AJNR Am J Neuroradiol*. 2013;34(3):533–540.
2. Tejada Neyra MA, Neuberger U, Reinhardt A, et al. Voxel-wise radiogenomic mapping of tumor location with key molecular alterations in patients with glioma. *Neuro Oncology*. 2018;20(11):1517–1524.
3. Qi S, Yu L, Li H, et al. Isocitrate dehydrogenase mutation is associated with tumor location and magnetic resonance imaging characteristics in astrocytic neoplasms. *Oncol Lett*. 2014;7(6):1895–1902.
4. Bates E, Wilson SM, Saygin AP, et al. Voxel-based lesion-symptom mapping. *Nat Neurosci*. 2003;6(5):448–450.
5. Wang YY, Zhang T, Li SW, et al. Mapping p53 mutations in low-grade glioma: a voxel-based neuroimaging analysis. *AJNR Am J Neuroradiol*. 2015;36(1):70–76.
6. Yuan Y, Yunhe M, Xiang W, et al. Mapping genetic factors in high-grade glioma patients. *Clin Neurol Neurosurg*. 2016;150:159–163.
7. Kimberg DY, Coslett HB, Schwartz MF. Power in voxel-based lesion-symptom mapping. *J Cogn Neurosci*. 2007;19(7):1067–1080.
8. Herbet G, Lafargue G, Duffau H. Rethinking voxel-wise lesion-deficit analysis: a new challenge for computational neuropsychology. *Cortex*. 2015;64:413–416.
9. Mah YH, Husain M, Rees G, Nachev P. Human brain lesion-deficit inference remapped. *Brain*. 2014;137(Pt 9):2522–2531.
10. Incekara F, van der Voort SR, Dubbink HJ, et al. Topographical mapping of 436 newly diagnosed IDH wildtype glioblastoma with vs. without MGMT promoter methylation. *Front Oncol*. 2020;10:596.
11. Ellingson BM, Cloughesy TF, Pope WB, et al. Anatomic localization of O6-methylguanine DNA methyltransferase (MGMT) promoter methylated and unmethylated tumors: a radiographic study in 358 de novo human glioblastomas. *Neuroimage*. 2012;59(2):908–916.
12. Darlix A, Deverdun J, Menjot de Champfleur N, et al. IDH mutation and 1p19q codeletion distinguish two radiological patterns of diffuse low-grade gliomas. *J Neurooncol*. 2017;133(1):37–45.
13. Talairach J, Tournoux P. *Co-Planar Stereotaxic Atlas of the Human Brain: 3-Dimensional Proportional System: An Approach to Cerebral Imaging*. 1st ed. Stuttgart, Germany: Thieme; 1988.
14. Collins DL, Neelin P, Peters TM, Evans AC. Automatic 3D intersubject registration of MR volumetric data in standardized Talairach space. *J Comput Assist Tomogr*. 1994;18(2):192–205.
15. Lee JW, Wen PY, Hurwitz S, et al. Morphological characteristics of brain tumors causing seizures. *Arch Neurol*. 2010;67(3):336–342.
16. Bullmore ET, Suckling J, Overmeyer S, Rabe-Hesketh S, Taylor E, Brammer MJ. Global, voxel, and cluster tests, by theory and permutation, for a difference between two groups of structural MR images of the brain. *IEEE Trans Med Imaging*. 1999;18(1):32–42.
17. Smith SM, Nichols TE. Threshold-free cluster enhancement: addressing problems of smoothing, threshold dependence and localisation in cluster inference. *Neuroimage*. 2009;44(1):83–98.
18. Manly BJF. *Randomization and Monte Carlo Methods in Biology*. London, UK: Chapman and Hall, 1991.
19. Subramanian A, Tamayo P, Mootha VK, et al. Gene set enrichment analysis: a knowledge-based approach for interpreting genome-wide expression profiles. *Proc Natl Acad Sci USA*. 2005;102(43):15545–15550.
20. Liu Y, Stojadinovic S, Hrycushko B, et al. Automatic metastatic brain tumor segmentation for stereotactic radiosurgery applications. *Phys Med Biol*. 2016;61(24):8440–8461.
21. Huttenlocher DP, Klauderman GA, Rucklidge WJ. Comparing images using the Hausdorff-distance. *IEEE Trans Patt Anal Machine Intel*. 1993;15:850–863.
22. Wang Y, Qian T, You G, et al. Localizing seizure-susceptible brain regions associated with low-grade gliomas using voxel-based lesion-symptom mapping. *Neuro Oncology*. 2015;17(2):282–288.
23. Cayuela N, Simó M, Majós C, et al. Seizure-susceptible brain regions in glioblastoma: identification of patients at risk. *Eur J Neurol*. 2018;25(2):387–394.
24. Zhang B, Chang K, Ramkissoon S, et al. Multimodal MRI features predict isocitrate dehydrogenase genotype in high-grade gliomas. *Neuro Oncology*. 2017;19(1):109–117.
25. Stockhammer F, Misch M, Helms HJ, et al. IDH1/2 mutations in WHO grade II astrocytomas associated with localization and seizure as the initial symptom. *Seizure*. 2012;21(3):194–197.
26. Wang Y, Zhang T, Li S, et al. Anatomical localization of isocitrate dehydrogenase 1 mutation: a voxel-based radiographic study of 146 low-grade gliomas. *Eur J Neurol*. 2015;22(2):348–354.
27. Jacques TS, Swales A, Brzozowski MJ, et al. Combinations of genetic mutations in the adult neural stem cell compartment determine brain tumour phenotypes. *EMBO J*. 2010;29(1):222–235.
28. Mueller W, Hartmann C, Hoffmann A, et al. Genetic signature of oligoastrocytomas correlates with tumor location and denotes distinct molecular subsets. *Am J Pathol*. 2002;161(1):313–319.
29. Labussière M, Idbaih A, Wang XW, et al. All the 1p19q codeleted gliomas are mutated on IDH1 or IDH2. *Neurology*. 2010;74(23):1886–1890.
30. Metellus P, Coulibaly B, Colin C, et al. Absence of IDH mutation identifies a novel radiologic and molecular subtype of WHO grade II gliomas with dismal prognosis. *Acta Neuropathol*. 2010;120(6):719–729.
31. Bardella C, Al-Dalahmah O, Krell D, et al. Expression of Idh1R132H in the murine subventricular zone stem cell niche recapitulates features of early gliomagenesis. *Cancer Cell*. 2016;30(4):578–594.
32. Waitkus MS, Diplas BH, Yan H. Biological role and therapeutic potential of IDH mutations in cancer. *Cancer Cell*. 2018;34(2):186–195.
33. Noushmehr H, Weisenberger DJ, Diefes K, et al. Identification of a CpG island methylator phenotype that defines a distinct subgroup of glioma. *Cancer Cell*. 2010;17(5):510–522.
34. Foulon C, Cerliani L, Kinkingnehun S, et al. Advanced lesion symptom mapping analyses and implementation as BCBtoolkit. *GigaScience*. 2018;7(3):1–17.
35. Zhang Y, Kimberg DY, Coslett HB, Schwartz MF, Wang Z. Multivariate lesion-symptom mapping using support vector regression. *Hum Brain Mapp*. 2014;35(12):5861–5876.